Investigation into stabilizing effect of the Z=82 shell closure against fission

S. Nath[1,2*]
[1] *Inter University Accelerator Centre, Aruna Asaf Ali Marg, New Delhi 110067, India and*
[2] *Department of Nuclear Physics, Andhra University, Visakhapatnam 530003, India*

Role of the $Z = 82$ shell closure in stabilizing the evaporation residues (ERs), produced in heavy ion-induced complete fusion reactions, against fission was investigated. Three experiments were performed at the Inter University Accelerator Centre (IUAC) to measure ER excitation function, ER-gated compound nucleus (CN) angular momentum distribution and fission fragment (FF) mass distribution for the reaction ^{19}F+^{184}W. Comparison of data from these experiments with data from other neighbouring systems having nearly similar entrance channel mass asymmetry indicated that instability set in after crossing of the $Z = 82$ shell in the CN.

1. Introduction

Extending the limit of the periodic table of elements has been an area of intense theoretical and experimental investigation for the last few decades [1, 2]. Existence of a doubly magic spherical nucleus beyond the limit dictated by bulk properties is dependent solely upon microscopic stabilization through shell effects. Following the first prediction [3], location of the trans-lead spherical nucleus was believed to be at $Z = 114$ and $N = 184$. Subsequently, however, different theoretical predictions for double shell closure beyond lead have been made and, in particular, proton shell with $Z = 114, 120, 122, 124, 126$ have been predicted. In the experimental front, the heaviest nuclei synthesized so far are ^{293,294}*117* [4] and ^{294}*118* [5]. Though these discoveries declare mankind's arrival on the *island of stability*, nothing conclusive can be said about the exact location of the doubly magic spherical superheavy nucleus yet. Given this scenario, it is left to experiments to search for the location of the same.

The formation cross sections of superheavy nuclei are so small (< 1 pb) that it is practically impossible to undertake systematic investigations of the reaction mechanism with the prevailing limits of experimental sensitivity. However, one can study the reaction mechanism near the heaviest doubly magic spherical nucleus available in nature, *viz.* $^{208}_{82}$Pb$_{126}$. The experimental signatures of the $Z = 82$ proton shell closure and the $N = 126$ neutron shell closure are of special interest, particularly towards the formation of a stable / long-lived ER. Knowledge acquired about the stabilizing effect of these two shells against fission might then be extrapolated to the next heavier proton and neutron shell closures.

Vermeulen *et al.* [6] carried out the first comprehensive study to verify the *expected* reduction of the fission competition in the deexcitation process of the CN due to the stabilizing influence of the strong ground-state shell effect near $N = 126$. ER cross sections were measured for ^{40}Ar-induced fusion reactions on ^{165}Ho, ^{169}Tm, ^{171}Yb, ^{174}Yb, ^{175}Lu, ^{176}Hf, ^{177}Hf, ^{178}Hf, ^{179}Hf, ^{180}Hf and ^{181}Ta targets. Standard statistical model calculation was performed for these reactions using the code HIVAP [7]. It was obseved that the maxima of the reduced cross sections for $4n$ evaporation channels leading to Th isotopes decreased monotonically with decreasing neutron number and there was no *structure* near $N = 126$. The results, thus, revealed *surprisingly* low stabilizing influence of the $N = 126$ spherical shell against fission competition.

The lack of stabilization against fission around $N = 126$ nuclei was explained [8] by the influence of collective excitations in terms

*Electronic address: subir@iuac.res.in

of a reduced collective contribution to the level density in spherical nuclei. Later Junghans *et al.* [9] analysed the measured production cross sections of ^{238}U projectile fragments in the vicinity of the $N = 126$ shell. The *expected* stabilization against fission for spherical nuclei near $N = 126$ was not found again. However, with the inclusion of collective enhancement in the level density (CELD) the experimental data were well described.

Ackermann [10] suggested that the $Z = 82$ shell closure might enhance the survival probability of the CN, formed in a heavy ion-induced fusion reaction, against fission which would result in enhanced ER cross sections. Andreyev *et al.* [11] studied the cross section systematics for the neutron-deficient nuclides $^{184-192}$Bi ($Z = 83$) and $^{186-192}$Po ($Z = 84$) produced in complete fusion reactions. A satisfactory description of the experimentl data in the long chains of Po and Bi isotopes required up to 35% reduction of the theoretical fission barriers used in the statistical model. This work suggested *strongly* increased fissility above the shell closure at $Z = 82$. Sagaidak *et al.* [12] further investigated fission barriers for Po nuclei produced in complete fusion reactions leading to $^{194-210}$Po CN. The search for the manifestation of CELD of deexciting Po nuclei was not successful in this study. The gradual drop in the production cross sections of Po nuclei in going from spherical shape with $N = 126$ to well-deformed ones with $N < 110$, which was reflected in the decrease in the macroscopic component of fission barriers, did not correspond to the expectations related to the collective excitations and deformation of nuclei involved in a CN deexcitation.

The present work aimed to study the melting away of the shell closure effects, if any, beyond $Z = 82$. Complete fusion of ^{19}F with ^{184}W leading to the formation of CN $^{203}_{83}$Bi$_{120}$, which has one extra proton beyond the $Z = 82$ shell closure, and its subsequent decay were studied. Three separate experiments were performed to measure ER excitation function, ER-gated CN angular momentum distribution and FF mass distribution. Data from these experiments were then compared with data from few other neighbouring systems, taken from the literature, having nearly similar entrance channel mass asymmetry to bring out the stabilizing influence of the $Z = 82$ shell closure against fission.

2. The experiments

Pulsed ^{19}F beam, in the laboratory energy range of 80 –130 MeV, was delivered by the 15UD Pelletron accelerator at the IUAC, New Delhi. The target was 210 μg/cm^2 thick ^{184}W [13] with a 110 μg/cm^2 thick carbon backing.

In the first experiment, ERs were separated from intense primary beam background by the Heavy-Ion Reaction Analyzer (HIRA) [14] and were transported to its focal plane. A schematic of the HIRA is shown in Fig. 1. Two silicon detectors were installed inside the sliding-seal scattering chamber at $\pm 24^\circ$ to measure Rutherford-scattered beam particles for absolute normalization of ER cross sections. A 35 μg/cm^2 carbon foil was placed 10 cm downstream from the target to reset the charge state of ERs. At the focal plane of the HIRA, a two-dimensional position-sensitive silicon detector with active area of 50 mm $\times$ 50 mm was used to detect ERs. The ERs were unambiguously identified (Fig. 2) by simultaneous measurement of their energy at the focal plane and time of flight (TOF) over the flight path of the HIRA (8.82 m). Characteristic γ-rays emitted by the ERs were recorded in singles and in coincidence, using a high-purity germanium (HPGe) detector, to measure transmission efciency of ERs through the HIRA. More details about the experiment can be obtained from Ref. [16].

In the second experiment, also performed in the HIRA, a multiplicity filter consisting of 14 Bismuth Germanate ($Bi_4Ge_3O_{12}$, in short BGO) crystals was placed around the target to detect γ-rays emitted by the ERs. Method of detection and identification of ERs were identical to those of the first experiment. For constructing γ-fold distribution, 14 time-to-digital converter (TDC) signals were recorded with ER arrival time at the focal plane as the common start and individual BGO timing sig-

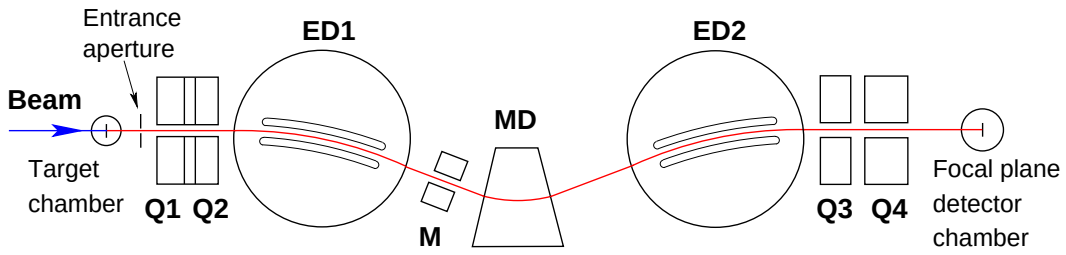

FIG. 1: Schematic of the HIRA. Q, ED, M and MD stand for magnetic quadrupole, electrostatic dipole, magnetic multipole and magnetic dipole, respectively.

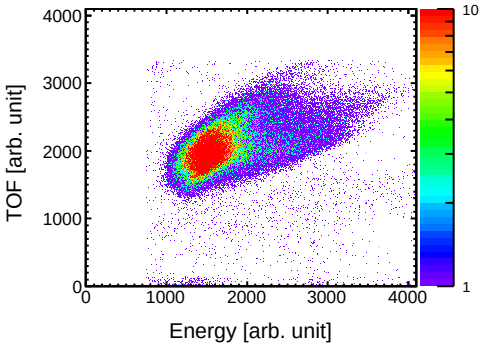

FIG. 2: Unambiguous identification of ERs from scattered beam particles on the basis of energy and TOF for the reaction ^{19}F+^{184}W at $E_{\rm lab}$ = 99.2 MeV. The plot was produced using ROOT [15].

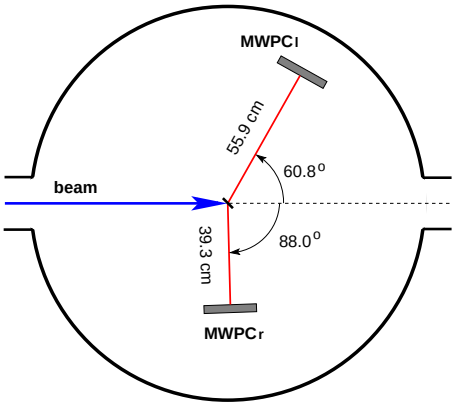

FIG. 3: Schematic of the experimental set up used for FF mass distribution measurement.

nals as the stop. Further details of the experiment can be found in Ref. [17].

The third experiment, detailes of which were presented in Ref. [18], was performed in the general purpose scattering chamber (GPSC) of the IUAC. A schematic of the experimental set up is shown in Fig. 3. Two multi-wire proportional counters (MWPCs) [19], mounted on the two rotatable arms of the GPSC and kept at folding angles, were used to detect the FFs in coincidence. Position information of the FFs was obtained from the delay-line readout of the wire planes. The fast timing signals from the anodes of the two MWPCs were used to obtain the FF time of flight with respect to the beam pulse. A fast coincidence between any of the anode signals and the radio frequency (RF) pulse was used as the master trigger for data acquisition. Analysis of data was performed using the IUAC's in-house data acquisition and analysis software CANDLE [20].

3. Data analysis and results

The total ER cross sections were calculated by the following relation

$$\sigma_{\rm ER} = \frac{Y_{\rm ER}}{Y_{\rm norm}} \left(\frac{d\sigma}{d\Omega}\right)_{\rm Ruth} \Omega_{\rm norm} \frac{1}{\epsilon_{\rm HIRA}} \quad (1)$$

where $Y_{\rm ER}$ is the number of ERs detected at the focal plane of the HIRA, $Y_{\rm norm}$ is the number of scattered beam particles detected by any of the normalization detectors, $\left(\frac{d\sigma}{d\Omega}\right)_{\rm Ruth}$ is the differential Rutherford scattering cross section in the laboratory system, $\Omega_{\rm norm}$ is the solid angle subtended by any of the normalization detectors and $\epsilon_{\rm HIRA}$ is the transmission

efficiency of the HIRA. Out of all these quantities on the right hand side of Eq. 1, $\epsilon_{\rm HIRA}$ contributes the maximum in overall error in the final cross sections and hence calls for special attention.

$\epsilon_{\rm HIRA}$ is a complex function of several parameters [16]. In the first experiment, it was measured by the ratio of counts of a specic γ-line in the coincidence spectrum to that in the singles spectrum for a specific ER channel at one energy. But, the same would be different for different exit channels and at different energies. A semi-microscopic Monte Carlo code was developed to calculate transmission efficiency of recoil separators (TERS) [21–23] and the same was used to calculate $\epsilon_{\rm HIRA}$. TERS generated *realistic* values of ER parameters, viz. displacement (position), divergence (angle), energy and charge states, event by event, and calculated ER trajectories through the HIRA by first-order ion optical transfer matrices. $\epsilon_{\rm HIRA}$ was then calculated by the ratio of number of ER trajectories reaching the focal plane to total number of trajectories. Very good agreement was achieved between the calculated and the measured transmission efficiency, in the case for which measurement was performed. For all other channels at different energies, TERS predictions were used to estimate ER cross sections.

Calculation of ER trajectories were performed assuming that their energy and charge states did not alter in-flight. Though this assumption is usually valid, presence of isomeric states in ERs can change the scenario significantly. An excited nucleus can come down to a lower excited state either by emitting a γ-photon or by internal conversion, as well as by other less probable avenues. In the latter process, one of the inner-orbital electrons receives the energy directly and is ejected from the atom, thus, altering the charge state of the ERs. A change in the charge state causes the ERs to follow a different trajectory inside the HIRA deviating from its journey toward the focal plane detector. Scrutinizing the structure of the ERs, it was found that several long-lived isomeric states existed in the ERs which could affect their transmission through

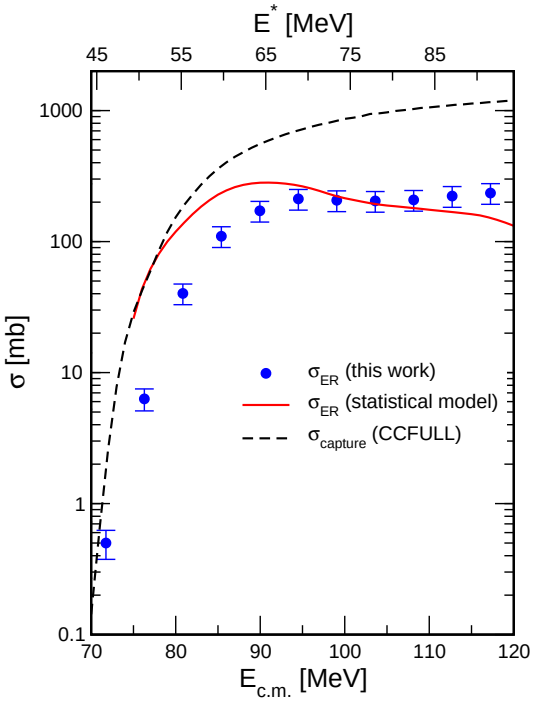

FIG. 4: Comparison between the experimental ER excitation function and statistical model calculation, obtained with $B_{\rm f}(0) = 10.2$ MeV, for the reaction ^{19}F+^{184}W. Capture cross sections calculated by the coupled-channels code CCFULL [24] are also shown.

the HIRA. However, calculation of internal conversion coefficients for the ERs established that measured cross sections would not be affected by the presence of these states beyond an excitation energy (E^*) of ∼65 MeV. ER cross sections, shown in Fig. 4, were finally determined with an overall error of ≤20% [16].

ER-gated γ-fold distributions were generated offline, from the 14 TDC signals recorded in the second experiment, using CANDLE. The first three moments of γ-multiplicity distribution viz. mean, variance and skewness, which are measures of central tendency, dispersion and degree of departure from symmetry respectively, were calculated following the formalism prescribed by Van Der Werf [25]. The γ-multiplicity distribution was assumed to be

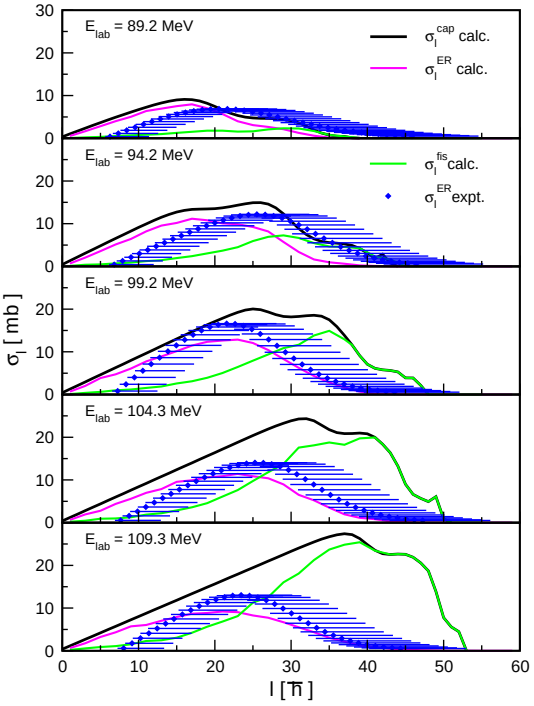

FIG. 5: Measured angular momentum distributions for the formation of ERs in the reaction ^{19}F+^{184}W. Capture cross sections from CCFULL and angular momentum distributions calculated using statistical model are also shown.

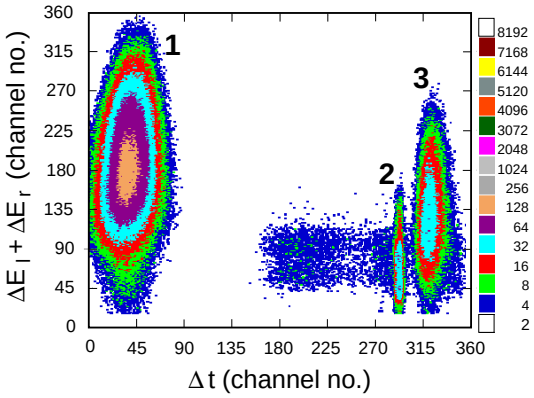

FIG. 6: Identification of different groups of events based on the timing and energy loss signals from the two MWPCs at the laboratory energy of 99.8 MeV. The group marked **1** represents events when two complimentary FFs were detected at the two detectors simultaneously. The group marked **2** denotes the elastic events detected only by the left MWPC. The group marked **3** indicates the events in which only one of the fragments was detected by the left MWPC.

described by a Fermi function, the shape of which was worked out by fitting two parameters to obtain the best fit for the experimentally observed γ-fold distribution. An *exact* method of reconstructing γ-multiplicity distribution, which can be applied under certain conditions, was also developed [26]. Finally, to get the CN angular momentum distribution for the formation of ERs (Fig. 5), average angular momentum removed by each non-statistical γ-ray was assumed to be $\sim 1.1\hbar$. Corrections due to angular momenta carried off by evaporated particles and statistical γ-rays were also incorporated [17].

In the fission experiment, coincident fission events were identified by the energy loss and timing signals from the two MWPCs (Fig. 6). Each fission event on the active area of the detectors was transformed to give the scattering angles with respect to the beam axis. Masses of the FFs were reconstructed by using the scattering angles and flight time difference of the complimentary FFs [27]. The electronic delay between the two timing signals was determined precisely at each beam energy assuming the condition of identity of the measured mass distributions in the two detectors and Viola systematics [28] for FF total kinetic energy. Measured mass distribution spectra (Fig. 7) were well described by Gaussians at all energy points.

4. Discussion

ER cross section for a fissile system, like the present one, can be factorized as follows [29]:

$$\sigma_{\rm ER} = \sigma_{\rm c}.P_{\rm CN}.W_{\rm sur}, \qquad (2)$$

where $\sigma_{\rm c}$ is the capture cross section, $P_{\rm CN}$ is CN formation probability and $W_{\rm sur}$ is fission survival probability of the CN. $\sigma_{\rm c}$ was calculated by CCFULL. $P_{\rm CN}$, dependent on non-compound processes such as quasifission [30], is the least known among the three factors.

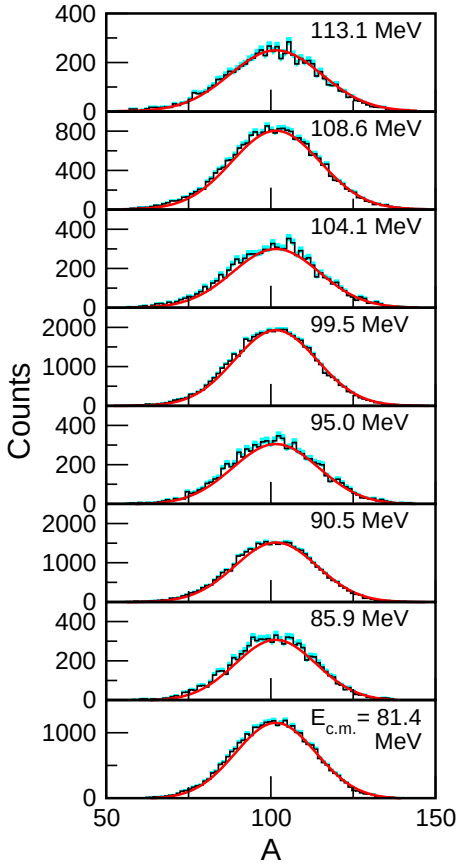

FIG. 7: Measured FF mass distribution (shown as histogram) for the system ^{19}F+^{184}W. Statistical errors are shown by shaded regions. The continuous line is the Gaussian fit at each energy.

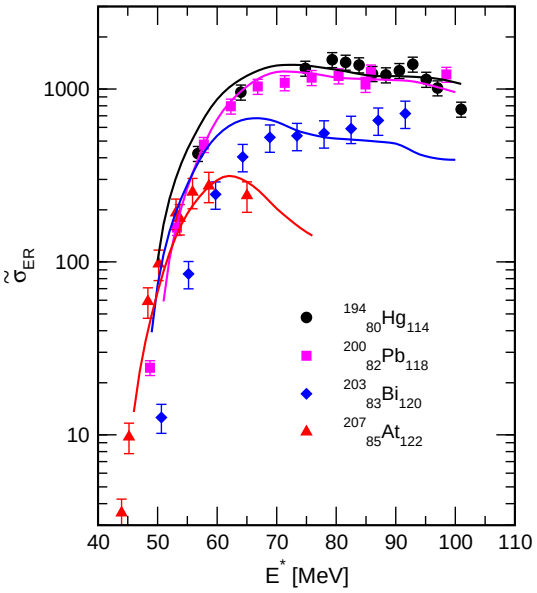

FIG. 8: Statistical model fits to the reduced ER cross sections ($\tilde{\sigma}_{\rm ER}$) for the ^{19}F-induced reactions leading to the CN ^{194}Hg, ^{200}Pb, ^{203}Bi and ^{207}At. Values of the respective $B_{\rm f}(0)$ are shown in the top panel of Fig. 9.

This quantity was ascertained indirectly from the FF mass distribution data. Variation of the standard deviation ($\sigma_{\rm m}$) and the variance ($\sigma^2_{\rm m}$) of the fitted Gaussian to the experimental FF mass distribution as a function of centre of mass energy ($E_{\rm c.m.}$) and the temperature of the fissioning CN, respectively, was studied [18]. Both $\sigma_{\rm m}$ and $\sigma^2_{\rm m}$ increased linearly with increase of the respective independent variable and did not show any *anomalous* behaviour. Based on these two observations, it was concluded that the present system proceeded towards the formation of CN after capture and non-compound processes were negligible. The ER cross sections were, thus, determined primarily by $W_{\rm sur}$. Measured cross sections were fitted with statistical model calculations [31] treating only the fission barrier for $\ell = 0$, $B_{\rm f}(0)$ as an adjustable parameter.

ER cross section data from three neighbouring systems viz. ^{19}F+^{175}Lu [32], ^{19}F+^{181}Ta [33, 34] and ^{19}F+^{188}Os [35] leading to the CN ^{194}Hg, ^{200}Pb and ^{207}At, respectively, were considered for comparison with the present data. Since all the four systems have very similar entrance channel mass asymmetry and they fall on the same side of the respective Businaro Gallone point [36], $P_{\rm CN}$ for these systems are expected to be quite similar. Thus, one can reliably compare the fission barriers, obtained by fitting experimental ER excitation function for different systems (Fig. 8). Statistical model calculation was carried out, and the best-fit value of $B_{\rm f}(0)$ was extracted for each system (Fig. 9). It was observed that the fitted value of $B_{\rm f}(0)$ for $Z = 82$

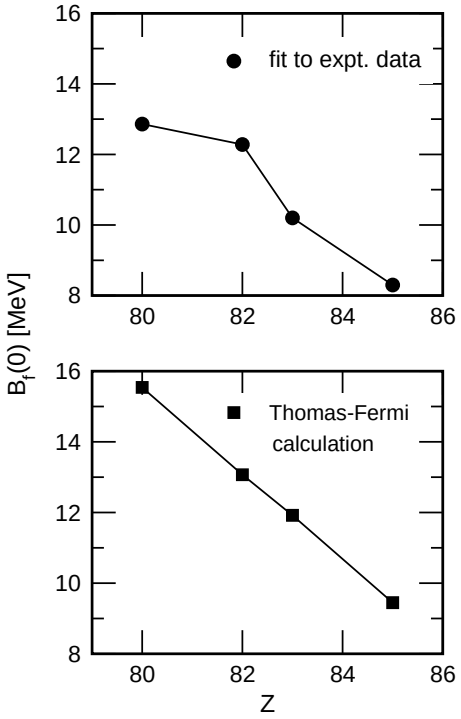

FIG. 9: Dependence of the fitted values of $B_{\rm f}(0)$ on atomic number of the CN for the systems shown in Fig. 8 (top panel) and the systematic (N, Z)-dependent $B_{\rm f}(0)$ for the same systems from Thomas-Fermi calculation (bottom panel).

was substantially enhanced, compared to its neighbours at $Z = 80$ and 83, than expected from its systematic (N, Z) dependence obtained from Thomas-Fermi calculation [37]. This enhancement was interpreted as being caused by the shell closure effect at $Z = 82$, which provides the additional stability against fission for ^{200}Pb.

Also, angular momentum distribution of the present system was compared with the same for the system ^{19}F+^{175}Lu $\rightarrow$ ^{194}Hg [32] in which the CN lies below the Z=82 shell (Fig. 10). It was observed that population of higher ℓ-values in the present system is less compared to the same in the system leading to the CN ^{194}Hg, at similar $\frac{E_{\rm c.m.}}{V_{\rm Coul.}}$ values, where $V_{\rm Coul.}$ is the Coulomb barrier. This observation also endorsed that the $Z = 82$ shell closure provides enhanced stability against fission and instability sets in after crossing of the shell at $Z = 82$.

It may be mentioned here that stabilizing effect of the Z=82 shell against fission can be better understood by studying excitation function and angular momentum distribution of individual ER channels. In the present work, total ER cross section and angular momentum distribution were measured. Formation of CN with the same neutron number (N) but with different atomic number (Z) scanning across $Z = 82$ can be considered in future experiments. Also, the effect of CELD in the vicinity of the $Z = 82$ and the $N = 126$ shells needs to be probed further.

Acknowledgments

This work was performed in collaboration with Gayatri Mohanto, J. Gehlot, K.S. Golda, A. Jhingan, T. Varughese, Dr. P. Sugathan, N. Madhavan, S. Muralithar (Inter University Accelerator Centre, New Delhi), Dr. P.V. Madhusudhana Rao (Andhra University, Visakhapatnam), Dr. E. Prasad (Calicut University, Calicut), Dr. Sunil Kalkal (Delhi University, Delhi), M.B. Naik, Dr. P.D. Shidling (Karnatak University, Dharwad), Jhilam Sadhukhan, Dr. Santanu Pal (Variable Energy Cyclotron Centre, Kolkata) and Dr. A.K. Sinha (UGC-DAE Consortium for Scientific Research, Kolkata). The author thanks the Pelletron staff of the IUAC for excellent operation of the accelerator during the experiments and Dr. A. Roy for many useful discussions.

References

[1] Yuri Oganessian, J. Phys. G **34**, R165 (2007).
[2] S. Hofmann and G. Münzenberg, Rev. Mod. Phys. **72**, 733 (2000).
[3] A. Sobiczewski, F.A. Gareev and B.N. Kalinkin, Phys. Lett. **22**, 500 (1966).
[4] Yu.Ts. Oganessian et al., Phys. Rev. Lett. **104**, 142502 (2010).
[5] Yu.Ts. Oganessian et al., Phys. Rev. C **74**, 044602 (2006).
[6] D. Vermeulen et al., Z. Phys. A, **318**, 157 (1984).

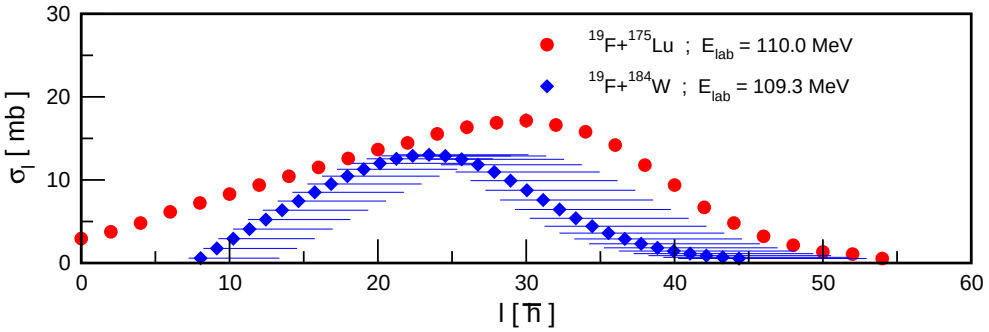

FIG. 10: Comparison of measured angular momentum distributions between the systems ^{19}F+^{175}Lu and ^{19}F+^{184}W at similar $\frac{E_{\rm c.m.}}{V_{\rm Coul.}}$.

[7] W. Reisdorf, Z. Phys. A **300**, 227 (1981).
[8] A.V. Ignatyuk, K.K. Istekov and G.N. Smirenkin, Yad. Fiz. **37**, 831 (1983).
[9] A.R. Junghans et al., Nucl. Phys. A **629**, 635 (1998).
[10] D. Ackermann et al., Eur. Phys. J. A **20**, 151 (2004).
[11] A.N. Andreyev et al., Phys. Rev. C **72**, 014612 (2005).
[12] R.N. Sagaidak and A.N. Andreyev, Phys. Rev. C **79**, 054613 (2009).
[13] P.D. Shidling et al., Nucl. Instrum. Methods A **590**, 79 (2008).
[14] A.K. Sinha et al., Nucl. Instrum. Methods A **339**, 543 (1994).
[15] http://root.cern.ch/drupal/.
[16] S. Nath et al., Phys. Rev. C **81**, 064601 (2010).
[17] S. Nath et al., Nucl. Phys. A **850**, 22 (2011).
[18] S. Nath et al., EPJ. Web. Conf. **17**, 16008 (2011).
[19] A. Jhingan et al., Rev. Sci. Instrum. **80**, 123502 (2009).
[20] E.T. Subramaniam, B.P. Ajith Kumar and R.K. Bhowmik, Collection and Analysis of Nuclear Data using Linux nEtwork, (unpublished).
[21] S. Nath, Nucl. Instrum. Methods A **576**, 403 (2007).
[22] S. Nath, Comput. Phys. Commun. **179**, 492 (2008).
[23] S. Nath, Comput. Phys. Commun. **180**, 2392 (2009).
[24] K. Hagino, N. Rowley and A.T. Kruppa, Comput. Phys. Commun. **123**, 143 (1999).
[25] S.Y. Van Der Werf, Nucl. Instrum. Methods **153**, 221 (1978).
[26] S. Nath, Nucl. Instrum. Methods A **640**, 225 (2011).
[27] R.K. Choudhury et al., Phys. Rev. C **60**, 054609 (1999).
[28] V.E. Viola, K. Kwiatkowski and M. Walker, Phys. Rev. C **31**, 1550 (1985).
[29] C.C. Sahm et al., Nucl. Phys. A **441**, 316 (1985).
[30] W.J. Swiatecki, Phys. Scr. **24**, 113 (1981).
[31] Gargi Chaudhuri and Santanu Pal, Phys. Rev. C **65**, 054612 (2002).
[32] S.K. Hui et al., Phys. Rev. C **62**, 054604 (2000).
[33] D.J. Hinde et al., Nucl. Phys. A **385**, 109 (1982).
[34] A.L. Caraley et al., Phys. Rev. C **62**, 054612 (2000).
[35] K. Mahata et al., Nucl. Phys. A **720**, 209 (2003).
[36] U.L. Businaro and S. Gallone, Nuovo Cimento **5**, 315 (1957).
[37] W.D. Myers and W.J. Swiatecki, Physical Review C **60**, 014606 (1999).